
Representation Disentanglement via Regularization by Identification

Juan Castorena^{* 1}

Abstract

This work focuses on the problem of learning disentangled representations from observational data. Given observations $\{\mathbf{x}^{(i)}\}_{i=1}^N$ drawn from $p(\mathbf{x}|\mathbf{y})$ with generative variables \mathbf{y} admitting the distribution factorization $p(\mathbf{y}) = \prod_c p(\mathbf{y}_c)$, we ask whether learning disentangled representations matching the space of observations with identification guarantees on the posterior $p(\mathbf{z}|\mathbf{x}, \hat{\mathbf{y}}_c)$ for each c , is plausible. We argue modern deep representation learning models are ill-posed with collider bias behaviour; a source of bias producing entanglement between generating variables. Under the rubric of causality, we show this issue can be explained and reconciled under the condition of identifiability; attainable under supervision or a weak-form of it. For this, we propose regularization by identification (ReI), a regularization framework defined by the identification of the causal queries involved in the learning problem. Empirical evidence shows that enforcing ReI in a variational framework results in disentangled representations equipped with generalization capabilities to out-of-distribution examples and that aligns nicely with the true expected effect between generating variables and measurement apparatus.

1. Introduction

One of the principal objectives of learning representations has been that of detecting/recognizing patterns or signatures of measurements to represent the qualitative and quantitative characteristics of the underlying physical processes being sensed. Most of the times sensing as dictated for example by the Nyquist rate (Shannon, 1948) acquires sufficient information for detection but leaves potentially unnecessary and redundant information on its measurements. Ideas to reduce such redundancies by representing information as concepts, patterns or features to achieve an economy of information have been the focus of study since its early days (Pearson, 1901a). Classical examples include principal component analysis (Pearson, 1901b) which assumes linear mapping functions along with orthogonality in its parametrizations. Independent component analysis (Bell & Sejnowski, 1995)

on the other hand, restricts the elements of the parametrizations to be independent using mutual information. However, both of these methods assume all measurements \mathbf{x} live in a low dimensional space, an assumption not applicable in all task contexts.

The standard variational formulation of representation learning frameworks consists in learning from the observables $\mathbf{x} \in \mathbb{R}^N$ a generative model $p_\theta(\mathbf{x}, \mathbf{z}) = p_\theta(\mathbf{x}|\mathbf{z})p_\theta(\mathbf{z})$ whose learned marginal likelihood $p_\theta(\mathbf{x})$ approximates the true $p_{\theta^*}(\mathbf{x})$. The latent variables $\mathbf{z} \in \mathbb{R}^N$ distributed as $p(\mathbf{z})$ and parameters $\theta \in \Theta$ are assumed unknown and focus on this problem has concentrated on finding priors that make the marginal and posterior $p_\theta(\mathbf{z}|\mathbf{x})$ tractable. Variational auto-encoders (VAE)'s (Kingma & Welling, 2013) for example, builds an efficient optimization approach that maximizes the conditional likelihood $p(\mathbf{x}|\mathbf{z})$ subject to similarity constraints quantified by the Kullback-Leibler (KL) divergence between a posterior approximate $q_\theta(\mathbf{z}|\mathbf{x})$ and a family of induced latent distribution priors $p_\theta(\mathbf{z})$ (typically an isotropic Gaussian). Problem with these group of methods for disentanglement is their focus on learning approximations of the true marginal data distributions without any restriction or guarantees on the prior in modeling the true generative mechanisms (Khemakhem et al., 2020). This not only disconnects meaning of the learned latent representations from supporting access to clear explanations and understanding (Lake et al., 2017) of the true generative processes, but also invokes problems of trust in their lack of robustness to out-of-distribution (OOD) examples (D'Amour et al., 2020) while keeping the necessary adjustments for diagnosis and repair (Szegedy et al., 2013) obscure (Pearl, 2019).

Recent trends (Bengio et al., 2013; Higgins et al., 2018; Locatello et al., 2019; Van Steenkiste et al., 2019; Khemakhem et al., 2020) are in consensus that disentanglement of the generating factors leads to increased robust representations that are less susceptible to the appearance of subsets of entangled factor variables in the intended tasks. Recent efforts along this line of work, includes unsupervised learning methods that exploit the enormous amounts of data available without the requirement of labels for each generating factor. Among the most popular methods includes β -VAE (Higgins et al., 2016), Annealed VAE (Burgess et al., 2018), Factor VAE (Kim & Mnih, 2018), DIP-VAE (Kumar et al., 2018) all imposing specific structure in the latent prior through

modifications of the KL term. The β -VAE (Higgins et al., 2016) for example includes a β scalar that controls the strength enforcing the latent prior. Increasing this scalar promotes the structure of the prior at the cost of divergence from the true marginal likelihood, thus β being a balancing term. Rooted in the concept of model identifiability, (Locatello et al., 2019) however, challenged the line of work of unsupervised learning disentanglements as impossible.

Weakly-supervised learning methods on the other hand have exploited weak-labels as they have shown to facilitate some form of disentanglement. (Mitrovic et al., 2020) proposes a method that consists in learning representations explaining the causal data generation mechanisms by promoting invariance to augmented data transformations, this under the principle of independent causal mechanism (Peters et al., 2016; 2017). Invariant risk minimization (IRM) of (Arjovsky et al., 2019) seeks for representations that produce predictions invariant to environment contexts. (Bouchacourt et al., 2018) seeks to learn representations by grouped observations (i.e., a factor of variation shared between observations within a group) and proposes a multi-level VAE for learning group representations and tackle the limitations of VAE’s assuming i.i.d observations. (Locatello et al., 2020) shows that disentangled representations can be obtained under weak-supervision when pairs of measurements share a factor of variation. Their approach modifies the β -VAE objective by enforcing similarities between the shared generative factors of variation and a decoupling of those uncommon. Worth noting is (Träuble et al., 2021), whose findings depict the method’s capability to also disentangle when training in datasets constructed by unknown correlations between the generative factors (i.e., at least two factors that vary together) while being independent; a problem known to be one of the root causes affecting DL OOD robustness and fairness (D’Amour et al., 2020). Identifiable VAE (iVAE) (Khemakhem et al., 2020) proposes a method enabling a weak-form of model identification. The definition therein consists in finding models that for all \mathbf{x}, \mathbf{z} , $\forall \theta, \theta' : p_{\theta}(\mathbf{x}) = p_{\theta'}(\mathbf{x})$; in other words, find distinct θ and θ' for which the marginal data distributions are equal. This however, is done without using and testing (Pearl, 2009) the constraints readable from the graphical generative model.

In light of these problems, the breadth of work in this research focuses towards contributing methods that seek to reconcile the issue of entanglement in existing deep representation learning models. The contributions of this work can be summarized as:

- “Regularization by Identification” (ReI) a regularization method defined by identification of the causal queries (Pearl, 1995) involved in the learning problem. The identification criteria is anchored in analysis of directed acyclic graphs (DAG’s), which, clearly es-

tipulates the generative model assumed and adverts the conditions required for identification from observations valid under the DAG model. Derivation of ReI in a given learning problem applies the rules of the *do*-calculus of (Pearl, 1995) to delete, exchange actions for observations and provide the adjustments necessary to guarantee identification of the involved queries from observational data.

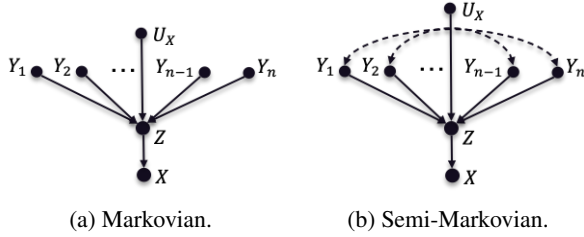
- We show under a pre-specified DAG model G encoding a typical data generative process, that standard representation learning frameworks present collider bias behaviour; a type of bias producing entanglement between the effects of the generating factors. An issue which has been either underlooked or not looked at all in representation learning to the best of our knowledge. For this, we reformulate the representation learning problem from a variational inference standpoint and derive under ReI the conditions that guarantee identification and that ultimately produce disentanglement.
- Provide empirical evidence that shows the potential of ReI in a dataset with joint variability between the generating factors; an issue recognized by (Träuble et al., 2021) as the problem of correlated data. In this case, ReI offers the potential to produce representations that: (1) disentangle the effects of the generating factors with results well aligned with true expected behavior (e.g., from like physics principles) supporting interpretation and understanding and (2) are more generalizable in the presence of out-of-distribution examples in comparison to the standard non-identifiable DL model counterparts.

2. Approach

2.1. Generative Model

Consider the problem of approximate posterior $p(\mathbf{z}|\mathbf{x}, \mathbf{y}_c)$ inference as in the VAE framework of (Kingma & Welling, 2013), with the distinction that unknown latent variable \mathbf{z} is conditioned on a generative factor \mathbf{y}_c . Measurements $\{\mathbf{x}^{(i)}\}_{i=1}^N$ are drawn from the marginal data distribution $p(\mathbf{x})$ generated by factor variables \mathbf{y} which admits factorizations of the form $p(\mathbf{y}) = \prod_c p(\mathbf{y}_c)$. The true posterior $p(\mathbf{z}|\mathbf{x}, \mathbf{y}_i)$ has powerful representational properties that if well approximated, can produce disentangled representations, remove potential sources of undesired spurious correlations, with better generalization possibilities to OOD cases while also provide clear paths for explaining and understanding the effects of the underlying generative mechanisms, a much needed requirement for scientific discovery.

In the variational inference framework this generative model can be encoded by the directed acyclic graph (DAG) G in Fig.1.

Figure 1: DAG G encoding generative process.

Variable $\mathbf{x} \in \mathbb{R}^M$ represents the sensor measurements, $\mathbf{y} \in \mathbb{R}^n$ with elements $y_c, c \in \{1, \dots, n\}$ are the ground truth generating factors (e.g., class membership scores), respectively. Sensor noise is denoted by the unmeasured $\mathbf{u}_x \in \mathbb{R}^M$ and $\mathbf{z} \in \mathbb{R}^M$ is a learned latent representation. Arrows emanating from y_c to \mathbf{z} , \mathbf{z} to \mathbf{x} are aligned with the causality of the generation mechanisms. In other words, there is causal precedence of the y_c 's and they are a direct cause (i.e., implied by the direct arrows between variables) of \mathbf{z} . Inspection of Fig. 1 reveals potential problems with the connections $\rightarrow \mathbf{z} \leftarrow$, indicative of a collider (Berkson, 1946; Kim & Pearl, 1983; Pearl, 2009); a source of potential bias. Conditioning on either the consequence \mathbf{z} or its descendant \mathbf{x} unblocks information flow from the causes $y_c \rightarrow \mathbf{z} \leftarrow y_j$ for $c \neq j$ in Fig. 1. For example, given that a restaurant is popular and service is bad, makes it more likely be due to good food. This collider bias phenomenon occurs as information on one of the causes makes the other causes involved more or less likely given that the consequence has occurred; even when the causes are independent (Pearl, 1995). In the variational framework, training by enforcing the likelihood term $p(\mathbf{x}|\mathbf{z})p(\mathbf{z}|\mathbf{y}_c)$ will, we argue open the free flow of information between the colliding generating factors y_c producing entangled representations if it remains untreated. Related works based on variational inference fundamentals like the VAE (Kingma & Welling, 2013) and even the supervised conditional VAE (Sohn et al., 2015) are susceptible to this collider problem when conditioning on \mathbf{z} as required by the likelihood function as no adjustment for the collider is provided. We recognize this as an important issue here and provide possible avenues for its resolution via the ReI framework while also providing connections to extend some of the analysis in identifiable based learning methods (Higgins et al., 2016; Locatello et al., 2020; Träuble et al., 2021) to integrate ReI in a modularized fashion.

2.2. Identification of Causal Effect Queries

Identification here sticks to Pearl's causal analysis framework (Pearl, 2009) to control/adjust for potential sources of bias (e.g., confounding, collider bias) between the participating variables. A DAG G (Pearl, 1995) (see Appendix A) encodes domain knowledge of the data generation mech-

anisms serves as a graphical tool to formulate the adjustments necessary for identification to control for bias or the free flow of information between variables with causally-unsupported dependencies. Identification of a causal query $p(y|\hat{x}) = p(y|do(X=x))$ enables inference of an intervention $do(X=x)$ from observed quantities alone and a model DAG G . Deriving such identifyability enables estimation of the quantities of interest unambiguously as G provides the model under which the distribution holds (Pearl, 1995). This, unlike nonidentifiable quantities which can only be defined ambiguously, and are likely to produce entangled representations. The VAE framework known to be very effective in approximating the marginal data distribution $p(\mathbf{x})$ does not provide any identifiable guarantees on the posterior distribution, rendering latent representations meaningless (in the sense of providing information about the true generative factors or its effects). Alternatively, the breadth of recent work most successful in representation disentanglement of the generative factors has relied in some form of identification (Peters et al., 2016; Bouchacourt et al., 2018; Mitrovic et al., 2020; Locatello et al., 2020; Khemakhem et al., 2020; Träuble et al., 2021).

In light of this discussion, we seek to lift the conventional usage of the approximate posterior $q(\mathbf{z}|\mathbf{x})$ in the VAE framework, for the causal query $p(\mathbf{z}|\mathbf{x}, \hat{y}_c)$ invoking intervention quantities of the $do(\mathbf{Y}_c = \mathbf{y}_c)$. Inspection of the assumed DAG G model in Fig. 1 adverts the presence of a collider. Adjustment for the participating variables in this collider is resolved by identification of the causal query $p(\mathbf{z}|\hat{y}_c)$ involved in the derivation of the posterior. This later (see Appendix B for full derivation) is given in Eq. (1) as:

$$p(\mathbf{z}|\hat{y}_c) = \sum_{\mathbf{w}_c} p(\mathbf{z}|\mathbf{y})p(\mathbf{w}_c) = \mathbb{E}_{p(\mathbf{w}_c)} [p(\mathbf{z}|\mathbf{y})] \quad (1)$$

where for easy of exposition, we denote the generating factors not in query by the set $\mathbf{w}_c = \{y_j : j \neq c\}$, with $\mathbf{y} = \mathbf{w}_c \cup \{y_c\}$. Note that the right hand side of Eq. (1) includes terms involving only standard probabilities obtained from observations. These as Eq. (1) implies can be computed by the expectation over the generating factors not in query of the conditional latent distribution.

Leaving one of the participating variables without control while conditioning on a collider unblocks the flow of information across the paths colliding at the common consequence. In the case of Fig. 1 for example, the query $p(\mathbf{z}|\hat{\mathbf{u}}_x)$ is unidentified as the factor \mathbf{u}_x is unmeasured and so the adjustment of Eq. (1) is not possible. Bias from the unmeasured \mathbf{u}_x under model G of Fig. 1 in the causal queries $p(\mathbf{z}|\hat{y}_c)$ will result in entanglement with the effects of $p(\mathbf{z}|\hat{\mathbf{u}}_x)$. Alternative remedies are in existence to mitigate this problem, but these have to rely on a parametrization enabling some form of approximation to $p(\mathbf{z}|\hat{\mathbf{u}}_x)$. When \mathbf{u}_x represents sensor noise for example, assumed to be stationary and un-

correlated with \mathbf{y} as depicted in the DAG model G of Fig.1, possibilities like the denoising methods of (Lehtinen et al., 2018; Laine et al., 2019) exist, which have shown to be highly effective.

2.3. Regularization by Identification

Regularization by identification (ReI) is a regularization engine defined by identification of the causal queries involved in the learning problem. Key step is that identification of the causal queries is anchored in analysis of a pre-specified DAG G model encoding the particular data generation mechanisms under which the identifications are valid. ReI reformulates traditional learning frameworks to make the necessary adjustments for causal identification of the involved queries; made explicit by regularization. This altogether different from the weakly-supervised setting of (Mitrovic et al., 2020; Peters et al., 2017; Arjovsky et al., 2019) which aim at finding the generating mechanisms by imposing some form of invariance to real or augmented data variability. Or to (Bouchacourt et al., 2018; Locatello et al., 2020) imposing invariance to shared generative factors between at least pairs of observations while keeping those detected as varying, free. In addition, distinct from (Khemakhem et al., 2020), our method relies on identification of the causal queries valid under a specified DAG G model rather than a statistical notion of model identification. Lastly, throughout this work the latent space lives in the same space as the observations (this made without restriction of analysis to latents living in lower dimensional spaces). This characteristic made in similarity with inverse denoising problems (Zhang et al., 2017; Lehtinen et al., 2018) and denoising diffusion models (Sohl-Dickstein et al., 2015; Ho et al., 2020) as examples. We assume this to yield representations more suitable to support interpretation, explanation and understanding of the effects of generating factors on data; as later verified empirically in Section 3.2.

The learning problem of the variational framework of (Kingma & Welling, 2013) optimizes the evidence lower bound (ELBO) to approximate the true posterior $p^*(\mathbf{z}|\mathbf{x})$ given measurements $\{\mathbf{x}^{(i)}\}_{i=1}^N$. The ELBO can be formulated by two terms: a likelihood $\mathcal{L}_\ell(\boldsymbol{\theta}, \boldsymbol{\phi}; \mathbf{x}^{(i)})$ and a regularizer $\mathcal{L}_\rho(\boldsymbol{\theta}, \boldsymbol{\phi}; \mathbf{x}^{(i)})$ as:

$$\mathcal{L}(\boldsymbol{\theta}, \boldsymbol{\phi}; \mathbf{x}^{(i)}) = \mathcal{L}_\ell(\boldsymbol{\theta}, \boldsymbol{\phi}; \mathbf{x}^{(i)}) - \lambda \mathcal{L}_\rho(\boldsymbol{\theta}, \boldsymbol{\phi}; \mathbf{x}^{(i)}) \quad (2)$$

where the likelihood term of most VAE flavors out there is given by Eq.(3) as:

$$\mathcal{L}_\ell(\boldsymbol{\theta}, \boldsymbol{\phi}; \mathbf{x}^{(i)}) = \mathbb{E}_{q(\mathbf{z}|\mathbf{x}^{(i)})} \left[\log p(\mathbf{x}^{(i)}|\mathbf{z}) \right] \quad (3)$$

and the regularizer $\mathcal{L}_\rho(\boldsymbol{\theta}, \boldsymbol{\phi}; \mathbf{x}^{(i)})$ given in case of the standard VAE by the Kullback-Leibler (KL) divergence

$$\mathcal{L}_\rho(\boldsymbol{\theta}, \boldsymbol{\phi}; \mathbf{x}^{(i)}) = D_{KL}(q(\mathbf{z}|\mathbf{x}^{(i)})||p(\mathbf{z})) \quad (4)$$

imposing a prior $p(\mathbf{z})$, typically a standard Gaussian, on the approximate posterior. The $\boldsymbol{\theta}, \boldsymbol{\phi}$ are the parameters of the encoder and decoder models, respectively, and optimized over the training dataset. The scalar λ in Eq.(2) is the regularizer strength balancing tradeoffs between the likelihood and priors, a parameter utilized by the β -VAE to promote the prior structure. Other extensions without identification guarantees, structuring the latent space by class under supervision is the conditional VAE of (Sohn et al., 2015) approximating instead, the conditional posterior $p(\mathbf{z}|\mathbf{x}, \mathbf{y})$ given data pairs $\{\mathbf{x}^{(i)}, \mathbf{y}^{(i)}\}_{i=1}^N$.

ReI reformulates the VAE, CVAE by lifting as in Section 2.2 the posterior $p(\mathbf{z}|\mathbf{x}, \mathbf{y})$ to the causal query $p(\mathbf{z}|\mathbf{x}, \hat{\mathbf{y}}_c)$. The reformulated posterior adjusted to render it identifiable under DAG G in Fig.1 is equivalent to:

$$p(\mathbf{z}|\mathbf{x}, \hat{\mathbf{y}}_c) = p(\mathbf{x}|\mathbf{z}) \mathbb{E}_{p(\mathbf{w}_c)} [p(\mathbf{z}|\mathbf{y})] / p(\mathbf{x}, \mathbf{y}_c) \quad (5)$$

involving the observables $\{\mathbf{x}^{(i)}, \mathbf{y}^{(i)}\}_{i=1}^N$. The adjustments in Eq.(5) block the flow of information between variables $\mathbf{y}_c \rightarrow \mathbf{z} \leftarrow \mathbf{w}_c$ when conditioning on \mathbf{z} , as required by the variational framework. The full derivation of Eq.(5) showing it an identifiable quantity can be referred to in Appendix B.

The adjustment of the ELBO made to reflect the causal query $p(\mathbf{z}|\mathbf{x}, \hat{\mathbf{y}}_c)$ instead of the standard posterior $p(\mathbf{z}|\mathbf{x}, \mathbf{y}_c)$. Derived in Appendix C, the adjustments required for identification of $p(\mathbf{z}|\mathbf{x}, \hat{\mathbf{y}}_c)$ results in the reformulated regularizer of the ELBO given in Eq.(6) as:

$$\mathcal{L}_\rho(\boldsymbol{\theta}, \boldsymbol{\phi}; \mathbf{x}^{(i)}, \mathbf{y}^{(i)}) = D_{KL} \left(q(\mathbf{z}|\mathbf{x}^{(i)}, \mathbf{y}_c^{(i)}) || \mathbb{E}_{p(\mathbf{w}_c)} \left[p(\mathbf{z}|\mathbf{y}^{(i)}) \right] \right) \quad (6)$$

Note that the necessary adjustments that render the causal query identifiable imposes constraints only on the ELBO regularizer. The likelihood function in learning problems remains, at least to the best of our knowledge, without modification in general. This is also consistent with the causal literature (Spirtes et al., 1996; Pearl, 2009) where free parameters abide to the likelihood function (e.g., least squares) while the adjustments imposed by identification constrain it (e.g., to be zero in the case of linear models (Spirtes, 1995)). Given these characteristics, we term our method ReI; as the constraints required to make the causal queries involved in the learning problem identifiable can be directly imposed by a regularizer. One of the motivating characteristics of ReI observed in the aforementioned reformulation of the ELBO is its modularity. This enables, the constraints imposed by ReI, like the regularizer derived in the VAE reformulation be added in a plug and play manner to other frameworks like (Higgins et al., 2016; 2018; Kim & Mnih, 2018; Bouchacourt et al., 2018; Locatello et al., 2020) similar to the work of (Venkatakrisnan et al., 2013) this last one focusing on regularizing denoisers.

In term of the functional encoder/decoder approximators, deep model capacity is assumed to satisfy the data processing inequality with equality constraints. In other words, the mutual information I between \mathbf{Y}_c and \mathbf{Z} is preserved relative to \mathbf{Y}_c and \mathbf{X} (i.e. $I(\mathbf{Y}_c, \mathbf{Z}) = I(\mathbf{Y}_c, \mathbf{X})$). This assumption has been used in other works (Locatello et al., 2020; Mao et al., 2022) and justified in the VAE’s objective to faithfully approximate the marginal data distribution.

2.4. Linear Parametrization

Parametrization of the encoding and decoding functionals $f_\theta(\mathbf{z}), h_\phi(\mathbf{x})$, respectively, imply interesting simplifications. In the simplest case assuming a linear model, in other words $f_\theta(\mathbf{z}) = \theta\mathbf{z}, h_\phi(\mathbf{x}) = \phi\mathbf{x}$ for example, simplifies adjustments of the type of Eq.(1) as these are equivalent to vanishing correlations. In a DAG G of disjoint variable sets X, Y, Z , a set S of correlation coefficients are set to zero or vanish (i.e., $\rho_{YX.Z} = 0$) if and only if X and Y are d -separated given set Z (Spirtes, 1995; Spirtes et al., 1996). Definitions of d -separation are included in Appendix A, but in summary, this is the fundamental tool to derive the conditions for identification of causal queries (Pearl, 1995). The adjustments in Eq.(1) thus imply in the linear parametrization constraining partial correlations between latent representations conditional on a given generating factor and those from others to zero in advance while keeping all others free (i.e., $r_{zy_c.\mathbf{w}_c} = 0$). One way of imposing these constraints is by parametrizing the regularizer in Eq.(6) which can be equipped with these restrictions through minimization of the partial correlations. However, as there are no guarantees with standard optimizers used in the DL world to attain vanishing partial correlations a better approach is to note that the vanishing partial correlations can be implemented via the orthogonal constraints.

$$\begin{aligned} (\tilde{\phi}\tilde{\theta})^T \tilde{\phi}\tilde{\theta} &= \mathbf{I} \\ \tilde{\phi} &= \prod_{d=D}^1 \phi_d, \quad \tilde{\theta} = \prod_{d=D}^1 \theta_d \end{aligned} \quad (7)$$

where \mathbf{I} is the identity matrix and the index order in d respects matrix multiplication order. Equipped with these constraints, the ELBO regularizer in the linear case restricts the free flow of information between the variables; preventing entanglement under the DAG G in Fig.1.

3. Experimentation

Experiments were conducted in applications of spectroscopic sensors, specifically using data from a laser induced breakdown spectroscopy (LIBS) instrument. LIBS is a remote sensing technology used for prediction of the chemical composition of geomaterials (e.g., rocks, soil) based on its signatures. On Mars, the ChemCam/SuperCam LIBS based

instruments are capable of investigating < 1 mm size samples by laser excited samples from up to 7m distances. It is equipped with a 1064nm laser and ultraviolet (UV), visible (VIO) and near infrared (NIR) band spectrometers; which altogether are capable of collecting the sample’s spectral signatures occurring between 240-905nm. It is through the analysis of such spectral signatures that chemical composition information of a sample can be readily extracted. Focus here, is applying the ReI framework directed towards three tasks: (1) representation disentanglement, (2) prediction and (3) transfer. First one consists in learning representations that characterize the spectral signatures of specific chemical elements. Second, uses the learning representations to predict chemical content of sampled materials while the third tests the generalization capabilities to dataset shifts by training from data collected in a controlled laboratory setting on Earth while deployment occurs in the wild on the Martian surface.

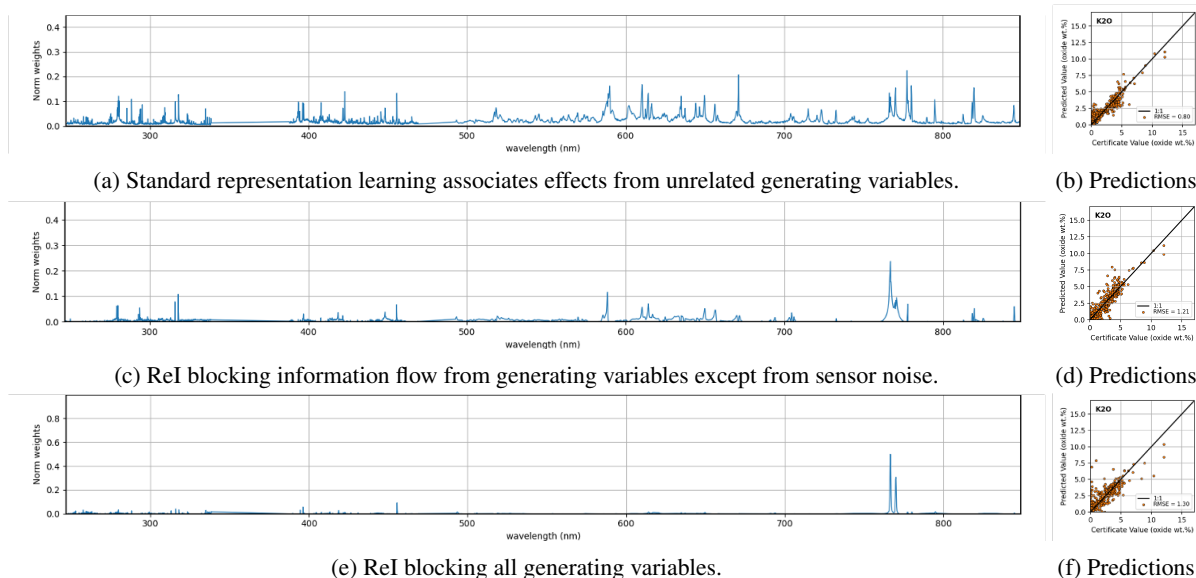
3.1. Dataset

The ChemCam LIBS instrument (Wiens et al., 2012) datasets contain raw and denoised spectra obtained from a variety of targets (e.g., rocks, soil) and from reference calibration standards of known and certified chemical composition. The specific datasets we employ consists of spectrally resolved LIBS signal measurements collected on Earth in a laboratory setting from a set of ~ 585 reference calibration standards (Clegg et al., 2017) and on Mars from a set of 10 reference standards of known true composition. Each target is repeatedly shot (e.g., 50 times) following each time measurements of the full 240-905 nm LIBS signal. After collection, wavelengths within the bands [240.811,246.635], [338.457,340.797], [382.13,387.859], [473.184,492.427], [849,905.574] were ignored out consistent with practices of the ChemCam team (Clegg et al., 2017).

3.2. Representation disentanglement

The abilities of ReI for learning disentangled representations were evaluated here. Training utilizes example pairs $\{\mathbf{x}^{(i)}, \mathbf{y}^{(i)}\}_{i=1}^N$ of LIBS signal \mathbf{x} measurements and corresponding chemical composition scores ground truth \mathbf{y} . Scores \mathbf{y}_c represent % oxide composition for $c \in \{1, \dots, 11\}$ indexing $\{\text{SiO}_2, \text{TiO}, \text{Al}_2\text{O}_3, \text{FeO}_T, \text{MgO}, \text{MnO}, \text{CaO}, \text{Na}_2\text{O}, \text{K}_2\text{O}, \text{CO}_2, \text{H}_2\text{O}\}$ and which altogether with sensor noise $\mathbf{u}_x \in \mathbb{R}^M$, produces the measured LIBS signal $\mathbf{x} \in \mathbb{R}^M$ with $M = 5485$.

For this, qualitative comparative evaluations of the produced representations from our ReI framework were performed in light of the known characteristic spectral response of each chemical oxide. We trained the VAE in an MLP architecture to produce representations which are compared in three cases: (1) the standard unidentified (causally-unconstrained),

Figure 2: Comparison of the learned representations for chemical oxide K_2O .

(2) constrained by ReI as in Eq.(2) with generating factors identified except for sensor noise \mathbf{u}_x and (3) ReI with all generating factors identified. Training uses the 585 reference calibration targets under leave one out while testing was done on data from the standard left out until all targets are covered. Hyperparameters of the DL model were set to an initial lr of 1.0, decayed after 75 epochs with cosine annealing (Loshchilov & Hutter, 2017) and with #epochs 300. Batches were constructed at each epoch from a set of 64 shot-averaged examples randomized over the whole training set without replacement. The shot-averages are computed by averaging the LIBS signal representations over an individual target and laser shot location. This averaging is consistent with common practices of the ChemCam team (Wiens et al., 2013; Clegg et al., 2017).

A representative example on the learned representations corresponding to chemical oxide K_2O is shown in Fig.2. These were generated by sampling from $q(\mathbf{z}|\mathbf{x}^{(i)}, \mathbf{y}_c^{(i)})$ by querying \mathbf{y}_c as K_2O and averaging over $L = 100$ samples. Figs.2a, 2c and 2e shows the learned representations for K_2O in: (1) standard causally-unconstrained, (2) ReI with sensor noise \mathbf{u}_x unidentified and (3) ReI with identification of all generating factors. The vertical axis of each plot shows the normalized magnitude and the horizontal axis represents spectral wavelength importance. Figs.2b, 2d and 2f illustrate the corresponding prediction performance $\tilde{\mathbf{y}}_c$ of the three cases using the representations \mathbf{z} along with a trained linear prediction head. Prediction performance by looking into point distribution along the 1:1 line and as measured by the root mean squared error (RMSE) shows similar performances in all three cases; with a marginal advantage of the standard VAE (i.e., (1) 0.8, (2) 1.21, (3)

1.30). However, these all come from distinct learned representations with key observations supporting evidence of collider behavior. First, note that K_2O (Potassium oxide) is known and expected to respond to wavelengths around $\sim 770\text{nm}$ as shown in Fig.3 illustrating the ground truth expected spectral responses of a variety of chemical elements. The standard VAE in Fig.2a resulted in a representation with spectral peaks deemed important spread throughout the entire spectrum. This is indicative of information flow between the generative causes $\mathbf{w}_c = \{y_j : j \neq c\}$ not in the query \mathbf{y}_c (i.e., K_2O) to \mathbf{y}_c from the unblocked paths $\mathbf{w}_c \rightarrow \mathbf{z} \leftarrow \mathbf{y}_c$ by conditioning on \mathbf{z} or its descendant \mathbf{x} . Fig.2c in contrast shows the resulting representation obtained by ReI with all generative factors except for sensor noise \mathbf{u}_x identified. Although most of the wavelengths previously deemed important were flattened, some spectral peak patterns from Fig.2a still persist although at a lower scale. This, we argue is indicative of the paths $\mathbf{w}_c \rightarrow \mathbf{z} \leftarrow \mathbf{u}_x$ and $\mathbf{u}_x \rightarrow \mathbf{z} \leftarrow \mathbf{y}_c$ producing information bridges between these variables. Finally, Fig.2e illustrates the representation by ReI with all generative factors identified. Note that in this case, most wavelengths were brought down to zero except for the two strong peaks at $\sim 770\text{nm}$. This, in alignment with the expected characteristic spectral response for K_2O as corroborated by Fig.3. Identification of the causal queries involved in the learning variational framework thus produced representations well aligned with the expected effects of the generating factors.

Empirical evidence provided thus supports our claim that DL models ill-suffer from collider bias. Although, as presented here in the prediction of in-distribution examples, downstream tasks can obscure the aforementioned illness,

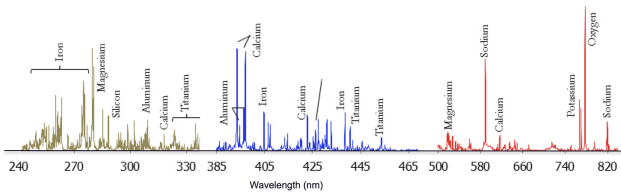


Figure 3: Known reference characteristic spectral response.

the task of representing the effects of generating factors; clearly shows evidence of this problem, with effects supporting collider behavior. These findings, thus provide a plausible alternative explanation to the spurious association problems between factors found in (Glocker et al., 2019; Geirhos et al., 2020; Pezeshki et al., 2021; Banerjee et al., 2021), to fairness (Zhao et al., 2017), and provide a venue for analysis and remediation through causality as viewed by (Pearl, 2010) and tackled here by ReI. We would like to note also that the learned representations from ReI visualized pictorially are amenable for interpretation, explain the effects of generating factors as they relate to the effects of the measuring apparatus, and can support understanding much needed for scientific discovery.

3.3. Prediction and Transfer

Quantitative evaluations that compared generalization in the prediction tasks of chemical composition of the learned representations in the presence of dataset shifts are evaluated here. The problem of dataset shifts originate within the scope of the LIBS application by training from data collections of LIBS measurements from targets on Earth in a laboratory setting while deployment occurs in data collections in the wild from Mars. (Clegg et al., 2017) found that the Martian environment has effects that shift the distribution of measurements in relationship to those on Earth and provided a manual engineered approach for its correction. This task then seeks to investigate the transferability of the representations in the presence of out-of-distribution shifts caused by deployment in a distinct environment.

Example representative results were included in Fig.4 which show ground truth versus prediction plots for two element oxides Al_2O_3 and MgO . Four leftmost Figs.4a,4e,4b,4f corresponds to performance results of the learned representation using standard VAE+FC linear head whereas the rightmost four Fig.4c,4g,4d,4h shows those from ReI. Figs. 4a,4e,4c,4g show that both standard and ReI present similar performance for in distribution example testing (under leave one out), with the standard being marginally better in RMSE. In contrast, Figs.4b,4f,4c,4g shows significant differences in performance for out-of-distribution (OOD) example testing. ReI presents better behaved performance and outperforms by larger margins compared to the standard in all cases.

Table 1: Transfer Performance Comparison

Architecture	RMSE (% oxide)
FC(10)	5.19
MLP(10)	5.06
MLPMixer(8)	5.23
ResNet(18) + FC(10)	6.23
U-Net +FC(5)	5.12
Transformer + FC(10)	6.12
VAE + FC(10)	4.51
ReI-VAE+FC(1)	2.45

Note that even though the standard methods present a performance advantage over ReI for in-distribution examples, that this is not the case for out-of-distribution examples collected in the wild from Mars. ReI learns representations with disentangled variables that show better generalizations against the tested out-of-distribution examples. This behavior, consistent with findings by (Tsipras et al., 2018) showing that highly predictive non-robust features in the data tend to reduce learner performance when presented with out-of-distribution examples.

3.4. DL model architectures at transfer

Table 1 provides additional results comparing performance on Earth-to-Mars transfer on a variety of DL architectures and averaged over all elements $y \in \mathbb{R}^n$ with $n = 11$. Comparisons include fully connected (FC), multilayer perceptron (MLP), MLP Mixer (Tolstikhin et al., 2021), ResNet (He et al., 2016), U-Net (Ronneberger et al., 2015), Transformers (Dosovitskiy et al., 2020) and again the standard VAE (Kingma & Welling, 2013). Note that some of the architectures do not produce a latent representation explicitly, these are however rather trained end-to-end for prediction. The number in parenthesis next to each architecture name (e.g., FC(10)) expresses the corresponding depth of layers. The results of Table 1 show that ReI outperforms standard architectures in cases of OOD examples regardless of the inductive biases implied by the architectural designs in comparison. Fig.5 shows instead transfer performance as a function of DL model depth. In this case, the FC, MLP, MLP Mixer and ResNet+FC networks were compared. This plot shows that ReI is capable of outperforming standard DL models which did not exhibit generalization capabilities to OOD cases regardless of depth in this case. As a final remark we would like to highlight that gains in task performance may not necessarily translate into more generalizable DL models. In fact, as evidenced by experiments, these may sometimes trick one’s belief of a better model. In our case, these issues were settled through experiments evaluating the resulting representations of the effects between the generating factors and the measuring apparatus and the

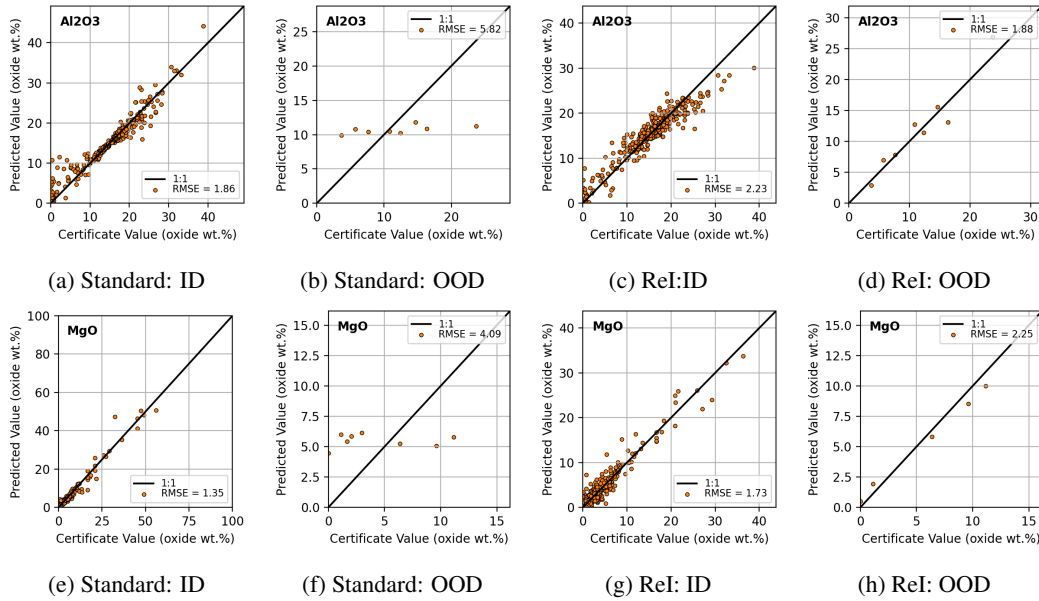


Figure 4: Performance comparison of the learned representations in out-of-distribution transfer.

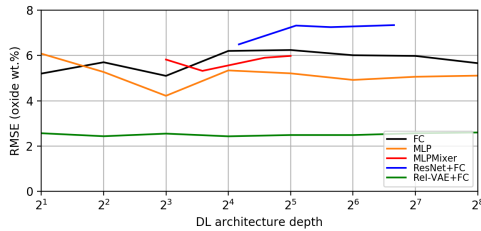


Figure 5: Transfer performance versus DL model depth.

expectations from domain knowledge.

4. Conclusions

In this work, we proposed ReI: a regularization method defined by the identification of causal queries anchored in analysis of graphical generative models of data. We argued that standard non-identifiable DL models are ill-biased by collider behaviour and showed supporting empirical evidence of this. In a variational framework, we showed how analysis of the graphical data generative model under the lens of causality can be used to adjust for collider bias via ReI in representation learning problems. Empirical evidence shows ReI is capable of learning the effects between the individual generating factors and the sensor, removing collider bias, producing representations in disentangled form, generalizable to OOD example cases and supporting interpretation, explanation and understanding of both factor effects and manipulations of these for sampling posterior generation.

References

- Arjovsky, M., Bottou, L., Gulrajani, I., and Lopez-Paz, D. Invariant risk minimization. *arXiv preprint arXiv:1907.02893*, 2019.
- Banerjee, I., Bhimireddy, A. R., Burns, J. L., Celi, L. A., Chen, L.-C., Correa, R., Dullerud, N., Ghassemi, M., Huang, S.-C., Kuo, P.-C., et al. Reading race: Ai recognises patient’s racial identity in medical images. *arXiv preprint arXiv:2107.10356*, 2021.
- Bell, A. J. and Sejnowski, T. J. An information-maximization approach to blind separation and blind deconvolution. *Neural computation*, 7(6):1129–1159, 1995.
- Bengio, Y., Courville, A., and Vincent, P. Representation learning: A review and new perspectives. *IEEE transactions on pattern analysis and machine intelligence*, 35(8): 1798–1828, 2013.
- Berkson, J. Limitations of the application of fourfold table analysis to hospital data. *Biometrics Bulletin*, 2(3):47–53, 1946.
- Bouchacourt, D., Tomioka, R., and Nowozin, S. Multi-level variational autoencoder: Learning disentangled representations from grouped observations. In *Proceedings of the AAAI Conference on Artificial Intelligence*, volume 32, 2018.
- Burgess, C. P., Higgins, I., Pal, A., Matthey, L., Watters, N., Desjardins, G., and Lerchner, A. Understanding disen-

- tangling in beta-vae. *arXiv preprint arXiv:1804.03599*, 2018.
- Clegg, S. M., Wiens, R. C., Anderson, R., Forni, O., Frydenvang, J., Lasue, J., Cousin, A., Payre, V., Boucher, T., Dyar, M. D., et al. Recalibration of the mars science laboratory chemcam instrument with an expanded geochemical database. *Spectrochimica Acta Part B: Atomic Spectroscopy*, 129:64–85, 2017.
- Dosovitskiy, A., Beyer, L., Kolesnikov, A., Weissenborn, D., Zhai, X., Unterthiner, T., Dehghani, M., Minderer, M., Heigold, G., Gelly, S., et al. An image is worth 16x16 words: Transformers for image recognition at scale. In *International Conference on Learning Representations*, 2020.
- D’Amour, A., Heller, K., Moldovan, D., Adlam, B., Alipanahi, B., Beutel, A., Chen, C., Deaton, J., Eisenstein, J., Hoffman, M. D., et al. Underspecification presents challenges for credibility in modern machine learning. *Journal of Machine Learning Research*, 2020.
- Geiger, D., Verma, T., and Pearl, J. d-separation: From theorems to algorithms. In *Machine Intelligence and Pattern Recognition*, volume 10, pp. 139–148. Elsevier, 1990.
- Geirhos, R., Jacobsen, J.-H., Michaelis, C., Zemel, R., Brendel, W., Bethge, M., and Wichmann, F. A. Shortcut learning in deep neural networks. *Nature Machine Intelligence*, 2(11):665–673, 2020.
- Glocker, B., Robinson, R., Castro, D. C., Dou, Q., and Konukoglu, E. Machine learning with multi-site imaging data: An empirical study on the impact of scanner effects. *arXiv preprint arXiv:1910.04597*, 2019.
- He, K., Zhang, X., Ren, S., and Sun, J. Deep residual learning for image recognition. In *2016 IEEE Conference on Computer Vision and Pattern Recognition (CVPR)*, pp. 770–778, 2016. doi: 10.1109/CVPR.2016.90.
- Higgins, I., Matthey, L., Pal, A., Burgess, C., Glorot, X., Botvinick, M., Mohamed, S., and Lerchner, A. beta-vae: Learning basic visual concepts with a constrained variational framework. 2016.
- Higgins, I., Amos, D., Pfau, D., Racaniere, S., Matthey, L., Rezende, D., and Lerchner, A. Towards a definition of disentangled representations. *arXiv preprint arXiv:1812.02230*, 2018.
- Ho, J., Jain, A., and Abbeel, P. Denoising diffusion probabilistic models. *Advances in Neural Information Processing Systems*, 33:6840–6851, 2020.
- Khemakhem, I., Kingma, D., Monti, R., and Hyvarinen, A. Variational autoencoders and nonlinear ica: A unifying framework. In *International Conference on Artificial Intelligence and Statistics*, pp. 2207–2217. PMLR, 2020.
- Kim, H. and Mnih, A. Disentangling by factorising. In *International Conference on Machine Learning*, pp. 2649–2658. PMLR, 2018.
- Kim, J. and Pearl, J. A computational model for causal and diagnostic reasoning in inference systems. In *International Joint Conference on Artificial Intelligence*, pp. 0–0, 1983.
- Kingma, D. P. and Welling, M. Auto-encoding variational bayes. *arXiv preprint arXiv:1312.6114*, 2013.
- Kumar, A., Sattigeri, P., and Balakrishnan, A. Variational inference of disentangled latent concepts from unlabeled observations. In *International Conference on Learning Representations*, 2018.
- Laine, S., Karras, T., Lehtinen, J., and Aila, T. High-quality self-supervised deep image denoising. *Advances in Neural Information Processing Systems*, 32, 2019.
- Lake, B. M., Ullman, T. D., Tenenbaum, J. B., and Gershman, S. J. Building machines that learn and think like people. *Behavioral and brain sciences*, 40, 2017.
- Lehtinen, J., Munkberg, J., Hasselgren, J., Laine, S., Karras, T., Aittala, M., and Aila, T. Noise2noise: Learning image restoration without clean data. *arXiv preprint arXiv:1803.04189*, 2018.
- Locatello, F., Bauer, S., Lucic, M., Raetsch, G., Gelly, S., Schölkopf, B., and Bachem, O. Challenging common assumptions in the unsupervised learning of disentangled representations. In *international conference on machine learning*, pp. 4114–4124. PMLR, 2019.
- Locatello, F., Poole, B., Rätsch, G., Schölkopf, B., Bachem, O., and Tschannen, M. Weakly-supervised disentanglement without compromises. In *International Conference on Machine Learning*, pp. 6348–6359. PMLR, 2020.
- Loshchilov, I. and Hutter, F. SGDR: Stochastic gradient descent with warm restarts. In *International Conference on Learning Representations*, 2017. URL <https://openreview.net/forum?id=Skq89Scxx>.
- Mao, C., Xia, K., Wang, J., Wang, H., Yang, J., Bareinboim, E., and Vondrick, C. Causal transportability for visual recognition. In *Proceedings of the IEEE/CVF Conference on Computer Vision and Pattern Recognition*, pp. 7521–7531, 2022.

- Mitrovic, J., McWilliams, B., Walker, J., Buesing, L., and Blundell, C. Representation learning via invariant causal mechanisms. *arXiv preprint arXiv:2010.07922*, 2020.
- Pearl, J. Causal diagrams for empirical research. *Biometrika*, 82(4):669–688, 1995.
- Pearl, J. *Causality*. Cambridge university press, 2009.
- Pearl, J. On measurement bias in causal inference. In *Proceedings of the Twenty-Sixth Conference on Uncertainty in Artificial Intelligence, UAI'10*, pp. 425–432, Arlington, Virginia, United States, 2010. AUAI Press. ISBN 978-0-9749039-6-5. URL <http://dl.acm.org/citation.cfm?id=3023549.3023599>.
- Pearl, J. The seven tools of causal inference, with reflections on machine learning. *Commun. ACM*, 62(3):54–60, February 2019. ISSN 0001-0782. doi: 10.1145/3241036. URL <http://doi.acm.org/10.1145/3241036>.
- Pearson, K. Liii. on lines and planes of closest fit to systems of points in space. *The London, Edinburgh, and Dublin philosophical magazine and journal of science*, 2(11): 559–572, 1901a.
- Pearson, K. Liii. on lines and planes of closest fit to systems of points in space. *The London, Edinburgh, and Dublin philosophical magazine and journal of science*, 2(11): 559–572, 1901b.
- Peters, J., Bühlmann, P., and Meinshausen, N. Causal inference by using invariant prediction: identification and confidence intervals. *Journal of the Royal Statistical Society: Series B (Statistical Methodology)*, 78(5):947–1012, 2016.
- Peters, J., Janzing, D., and Schölkopf, B. *Elements of causal inference: foundations and learning algorithms*. The MIT Press, 2017.
- Pezeshki, M., Kaba, O., Bengio, Y., Courville, A. C., Precup, D., and Lajoie, G. Gradient starvation: A learning proclivity in neural networks. *Advances in Neural Information Processing Systems*, 34, 2021.
- Ronneberger, O., Fischer, P., and Brox, T. U-net: Convolutional networks for biomedical image segmentation. In *International Conference on Medical image computing and computer-assisted intervention*, pp. 234–241. Springer, 2015.
- Shannon, C. E. A mathematical theory of communication. *The Bell system technical journal*, 27(3):379–423, 1948.
- Sohl-Dickstein, J., Weiss, E., Maheswaranathan, N., and Ganguli, S. Deep unsupervised learning using nonequilibrium thermodynamics. In *International Conference on Machine Learning*, pp. 2256–2265. PMLR, 2015.
- Sohn, K., Lee, H., and Yan, X. Learning structured output representation using deep conditional generative models. *Advances in neural information processing systems*, 28, 2015.
- Spirtes, P. Directed cyclic graphical representations of feedback models. In *Proceedings of the Eleventh conference on Uncertainty in artificial intelligence*, pp. 491–498, 1995.
- Spirtes, P., Richardson, T., Meek, C., Scheines, R., and Glymour, C. Using d-separation to calculate zero partial correlations in linear models with correlated errors. *Publisher: Carnegie Mellon University*, 1996.
- Szegedy, C., Zaremba, W., Sutskever, I., Bruna, J., Erhan, D., Goodfellow, I., and Fergus, R. Intriguing properties of neural networks. *arXiv preprint arXiv:1312.6199*, 2013.
- Tolstikhin, I. O., Houlsby, N., Kolesnikov, A., Beyer, L., Zhai, X., Unterthiner, T., Yung, J., Steiner, A., Keysers, D., Uszkoreit, J., et al. Mlp-mixer: An all-mlp architecture for vision. *Advances in Neural Information Processing Systems*, 34:24261–24272, 2021.
- Träuble, F., Creager, E., Kilbertus, N., Locatello, F., Dittadi, A., Goyal, A., Schölkopf, B., and Bauer, S. On disentangled representations learned from correlated data. In *International Conference on Machine Learning*, pp. 10401–10412. PMLR, 2021.
- Tsipras, D., Santurkar, S., Engstrom, L., Turner, A., and Madry, A. Robustness may be at odds with accuracy. In *International Conference on Learning Representations*, 2018.
- Van Steenkiste, S., Locatello, F., Schmidhuber, J., and Bachem, O. Are disentangled representations helpful for abstract visual reasoning? *Advances in Neural Information Processing Systems*, 32, 2019.
- Venkatakrishnan, S. V., Bouman, C. A., and Wohlberg, B. Plug-and-play priors for model based reconstruction. In *2013 IEEE Global Conference on Signal and Information Processing*, pp. 945–948. IEEE, 2013.
- Wiens, R., Maurice, S., Lasue, J., Forni, O., Anderson, R., Clegg, S., Bender, S., Blaney, D., Barraclough, B., Cousin, A., Deflores, L., Delapp, D., Dyar, M., Fabre, C., Gasnault, O., Lanza, N., Mazoyer, J., Melikechi, N., Meslin, P.-Y., Newsom, H., Ollila, A., Perez, R., Tokar, R., and Vaniman, D. Pre-flight calibration and initial data processing for the chemcam laser-induced breakdown spectroscopy instrument on the mars science laboratory rover. *Spectrochimica Acta Part B: Atomic Spectroscopy*, 82:1 – 27, 2013. ISSN 0584-8547. doi: <https://doi.org/10.1016/j.sab.2013.02>.

003. URL <http://www.sciencedirect.com/science/article/pii/S0584854713000505>.

Wiens, R. C., Maurice, S., Barraclough, B., Saccoccio, M., Barkley, W. C., Bell, J. F., Bender, S., Bernardin, J., Blaney, D., Blank, J., et al. The chemcam instrument suite on the mars science laboratory (msl) rover: Body unit and combined system tests. *Space science reviews*, 170(1):167–227, 2012.

Zhang, K., Zuo, W., Chen, Y., Meng, D., and Zhang, L. Beyond a gaussian denoiser: Residual learning of deep cnn for image denoising. *IEEE transactions on image processing*, 26(7):3142–3155, 2017.

Zhao, J., Wang, T., Yatskar, M., Ordonez, V., and Chang, K.-W. Men also like shopping: Reducing gender bias amplification using corpus-level constraints. In *Proceedings of the 2017 Conference on Empirical Methods in Natural Language Processing*, pp. 2979–2989, 2017.

A. Background

A.1. Directed acyclic graphs

In the language of causality, the data generation process of a measurement $\mathbf{x} \in \mathbb{R}^N$ is represented by a directed acyclic graph (DAG) (Pearl, 1995) with generating variables as nodes, directed edges expressing a causal relationship between variables and p inducing a distribution over variables. The Markov compatibility property for DAGs states that the joint distribution p is compatible with a DAG G or that G represents p if it admits the product decomposition

$$p(x_1, \dots, x_n) = \prod_i p(x_i | pa_i). \quad (8)$$

Variables pa_i are the Markovian parents of x_i that belong to the minimal set of predecessors of x_i that renders x_i independent of all its other predecessors; in other words that, $p(x_i | pa_i) = p(x_i | x_1, \dots, x_{i-1})$ (Pearl, 2010). Causal analysis of the DAG allows access to a clear picture of the model assumptions, enables analysis for identification of causal effects, diagnoses for potential sources of bias, and provides the means to repair for them.

A.2. *do*-calculus

d-Separation denoted by $X \perp\!\!\!\perp Y | \mathbf{Z}$ implies conditional independence of X and Y given a set of variables \mathbf{Z} in every distribution compatible with the DAG, while absence of *d*-Separation implies the converse; a dependence in almost all distributions compatible with the DAG (Geiger et al., 1990). In (Pearl, 1995), variables X and Y are *d*-Separated given Z if and only if Z blocks every path from node X to node Y . The two conditions of such blocking are:

- In the paths $i \rightarrow m \rightarrow j$ or $i \leftarrow m \rightarrow j$ the node m is in Z , or
- there is a collider $i \rightarrow m \leftarrow j$ where neither node m nor its descendant is in Z .

For a DAG G , $G_{\overline{X}}$ and $G_{\underline{X}}$ denote, respectively, the graphs obtained by deleting the incoming and outgoing arrows at node X . The rules of interventional calculus according to Pearl are given as (Pearl, 1995; 2010):

”**Rule 1** (Insertion/deletion of observations):

$$p(y, \hat{x}, z, w) = p(y, \hat{x}, w) \quad \text{if } (Y \perp\!\!\!\perp Z) | X, W)_{G_{\overline{X}}}$$

Rule 2 (Action/observation exchange):

$$p(y, \hat{x}, \hat{z}, w) = p(y, \hat{x}, z, w) \quad \text{if } (Y \perp\!\!\!\perp Z) | X, W)_{G_{\overline{XZ}}}$$

Rule 3 (Insertion/deletion of actions):

$$p(y, \hat{x}, \hat{z}, w) = p(y, \hat{x}, w) \quad \text{if } (Y \perp\!\!\!\perp Z) | X, W)_{G_{\overline{XZ}}}$$

These rules encompass the fundamental rules of the *do*-calculus (Pearl, 1995) enabling the identification of causal effects for expressions of the form $p(y | \hat{x})$ involving interventions \hat{x} ; which when identified reduce to an equivalent expression involving standard probabilities of observed quantities.

B. Identification of Causal Queries

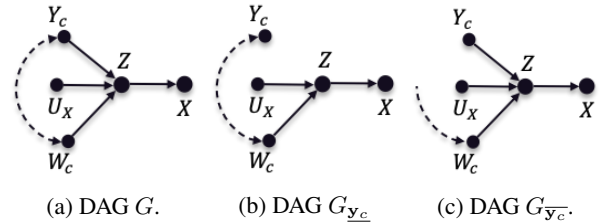


Figure 6: Simplified DAG

Derivation of the identification of causal effects $p(\mathbf{z} | \hat{\mathbf{y}}_c)$ in Eq.(1) entails using the rules of the *do*-calculus to convert probabilities of interventions to expressions involving only standard probabilities. For this, we make use of the DAGs shown in Fig.6 where we simplify the number of classes n indexed by c to only two for easy of exposition of the derivations but without restricting the generalization results to any number of n classes. The DAG in Fig.6a is the original generating model while Fig.6b removes edges of arrows that point outward and Fig.6c those that point inward of \mathbf{y}_c , respectively. Given that under the DAG $G_{\mathbf{y}_c}$, \mathbf{z} and \mathbf{y}_i are not *d*-Separated requires introducing additional conditioning on variables as follows. We would like to note, that in the presence of collider bias (i.e., when observing \mathbf{z} or its descendant \mathbf{x}) unblocking the information flow in paths $\mathbf{y}_c \rightarrow \mathbf{z} \leftarrow \mathbf{w}_c$, analysis of the DAG’s in Fig.6 becomes equivalent to that in Fig.1a.

Application of the law of total probability in Eq.(9) and the chain rule in Eq.(10) yields:

$$p(\mathbf{z}|\hat{\mathbf{y}}_c) = \sum_{\mathbf{w}_c} p(\mathbf{z}, \hat{\mathbf{y}}_c, \mathbf{w}_c)/p(\hat{\mathbf{y}}_c) \quad (9)$$

$$= \sum_{\mathbf{w}_c} p(\mathbf{z}|\hat{\mathbf{y}}_c, \mathbf{w}_c)p(\hat{\mathbf{y}}_c|\mathbf{w}_c)p(\mathbf{w}_c)/p(\hat{\mathbf{y}}_c) \quad (10)$$

$$= \sum_{\mathbf{w}_c} p(\mathbf{z}|\hat{\mathbf{y}}_c, \mathbf{w}_c)p(\mathbf{w}_c) \quad (11)$$

$$= \sum_{\mathbf{w}_c} p(\mathbf{z}|\mathbf{y})p(\mathbf{w}_c) = \mathbb{E}_{p(\mathbf{w}_c)} [p(\mathbf{z}|\mathbf{y})] \quad (12)$$

while Eq.(11) follows by definition of the *do* operator implying no effect on an intervention conditioned on any variables (i.e., $p(\hat{\mathbf{y}}_c|\mathbf{w}_c) = p(\hat{\mathbf{y}}_c)$). Eq.(12) is derived using the rules of *do*-calculus to test for *d*-Separations using Rule 2 for action/intervention exchange. Given that $(\mathbf{Z} \perp\!\!\!\perp \mathbf{Y}_c | \mathbf{W}_c)_{G_{\mathbf{y}_c}}$ is *d*-separated in $G_{\mathbf{y}_c}$ in Fig.6b (i.e., identifiable) allows the exchange from $p(\mathbf{z}|\hat{\mathbf{y}}_c, \mathbf{w}_c)$ to $p(\mathbf{z}|\mathbf{y}_c, \mathbf{w}_c)$ and since $\mathbf{y} = \mathbf{w}_c \cup \{\mathbf{y}_c\}$ by our definition, completes the proof. Extensions to cases with presence of more than two cases i, j , implies the DAG in Fig.1 in Sec 4. The results here, can be generalized to n by substituting \mathbf{w}_i for \mathbf{y}_j with $\mathbf{w}_i = \{\mathbf{y}_j : j \neq i\}$.

Abusing causal notation, we derive the identifiability conditions of the causal query $p(\mathbf{z}|\mathbf{x}, \hat{\mathbf{y}}_c)$ in Eq.5 noting that all terms involved respect the causal direction.

$$p(\mathbf{z}|\mathbf{x}, \hat{\mathbf{y}}_c) \quad (13)$$

$$= p(\mathbf{x}|\mathbf{z}, \hat{\mathbf{y}}_c)p(\mathbf{z}|\hat{\mathbf{y}}_c)p(\hat{\mathbf{y}}_c)/p(\mathbf{x}, \hat{\mathbf{y}}_c) \quad (14)$$

$$= p(\mathbf{x}|\mathbf{z}) \mathbb{E}_{p(\mathbf{w}_c)} [p(\mathbf{z}|\mathbf{y})] / p(\mathbf{x}, \mathbf{y}_c) \quad (15)$$

Eq.(14) follows by application of the chain rule of probability. Deletion of actions from $p(\mathbf{x}|\mathbf{z}, \hat{\mathbf{y}}_c)$ follows by applying Rule 3, satisfied when *d*-separation $(\mathbf{X} \perp\!\!\!\perp \mathbf{Y}_c | \mathbf{Z})_{G_{\mathbf{y}_c}}$ is satisfied. By inspection of Fig.6c we see this is indeed the case. Also, the action $p(\hat{\mathbf{y}}_c)$ is by definition one and substituting the result of the conditional latent distribution $p(\mathbf{z}|\hat{\mathbf{y}}_c)$ in Eq.(12) completes computing the numerator in Eq.(15) from observational data only. The denominator $p(\mathbf{x}, \hat{\mathbf{y}}_c)$ follows by adding \mathbf{z} through the law of total probability and using the chain rule as $\sum_{\mathbf{z}} p(\mathbf{x}, \hat{\mathbf{y}}_c|\mathbf{z})p(\mathbf{z})$. The action/observation exchange $\sum_{\mathbf{z}} p(\mathbf{x}, \mathbf{y}_c|\mathbf{z})p(\mathbf{z})$ then follows by checking if $(\mathbf{X} \perp\!\!\!\perp \mathbf{Y}_c | \mathbf{Z})_{G_{\mathbf{y}_c}}$ is satisfied; which is indeed the case by inspection of Fig.6b, completing the proof.

C. ELBO

Derivation of the ELBO in Eq.(2) follows the same steps as in (Kingma & Welling, 2013) starting with the Kullback-

Leibler (KL) divergence.

$$D_{KL}(q(\mathbf{z}|\mathbf{x}, \mathbf{y}_c)||p(\mathbf{z}|\mathbf{x}, \hat{\mathbf{y}}_c)) = - \sum q(\mathbf{z}|\mathbf{x}, \mathbf{y}_c) \log p(\mathbf{z}|\mathbf{x}, \hat{\mathbf{y}}_c)/q(\mathbf{z}|\mathbf{x}, \mathbf{y}_c) \quad (16)$$

$$= - \mathbb{E}_{q(\mathbf{z}|\mathbf{x}, \mathbf{y}_c)} \{ \log p(\mathbf{x}|\mathbf{z}) \} - \sum q(\mathbf{z}|\mathbf{x}, \mathbf{y}_c) \log \mathbb{E}_{p(\mathbf{w}_c)} [p(\mathbf{z}|\mathbf{y})] / q(\mathbf{z}|\mathbf{x}, \mathbf{y}_c) + \log p(\mathbf{x}, \mathbf{y}_c). \quad (17)$$

Eq.(16) follows by definition of the KL Leibler divergence, while Eq.(17) substitutes the result from the identification adjustments for the causal query $p(\mathbf{z}|\mathbf{x}, \hat{\mathbf{y}}_c)$ in Eq.(15). Based on Eq(17), the ELBO can be written as in Eq.(18), completing its derivation.

$$\log p(\mathbf{x}^{(i)}, \mathbf{y}_c^{(i)}) \geq \mathcal{L}(\boldsymbol{\theta}, \phi; \mathbf{x}^{(i)}, \mathbf{y}_c^{(i)}) = \mathbb{E}_{q(\mathbf{z}|\mathbf{x}^{(i)}, \mathbf{y}_c^{(i)})} \left\{ \log p(\mathbf{x}^{(i)}|\mathbf{z}) \right\} - D_{KL} \left(q(\mathbf{z}|\mathbf{x}^{(i)}, \mathbf{y}_c^{(i)}) || \mathbb{E}_{p(\mathbf{w}_c)} [p(\mathbf{z}|\mathbf{y}^{(i)})] \right). \quad (18)$$

In this proposal we focus on the problems of explainable and generalizable AI from a causal inference perspective. Standard DL frameworks have produced performances that are unquestionably among if not the best in many applications and tasks. However, their adoption in science has taken a slower pace as issues of explainability, interpretability and generalization are far from being solved. We argue, these problems can be resolved by integration of causal analysis and modern ML; where the former provides a formal mathematical language and analysis to encode application domain knowledge. Here, we propose Regularization by Identification (ReI): a regularization engine bridging application domain knowledge with the power of standard DL models in a modular fashion.